

Thermomechanical Analysis of Glass Powder Based Eco-concrete Panels: Limitations and Performance Evaluation

Abdelmoutalib Benfrid¹, Abdeldjalil Benbakhti², Zouaoui R. Harrat^{1*}, Mohammed Chatbi¹, Baghdad Krour¹, Mohamed Bachir Bouiadjra^{1,3}

¹ Laboratoire des Structures et Matériaux Avancés dans le Génie Civil et Travaux Publics, University of Djillali Liabes, 22000 Sidi Bel-Abbes, Algeria

² Department of Hydraulics-Institute of Technology, Maghnia University Center, 13000 Maghnia, Algeria

³ Thematic Agency for Research in Science and Technology, ATRST, 16000 Algiers, Algeria

* Corresponding author, e-mail: zouaoui.harrat@dl.univ-sba.dz

Received: 12 June 2022, Accepted: 11 July 2023, Published online: 31 July 2023

Abstract

This article presents a comprehensive investigation into the thermomechanical analysis of glass powder as an additive in concrete. The efficient Eshelby's model is utilized to determine the relevant composite properties, considering the spherical shape of the glass powder. A higher-order shear deformation plate theory is employed to theoretically simulate the reinforced concrete panel, ensuring accuracy and simplicity. Equilibrium equations are derived using the virtual work concept, and energy equations are derived using Hamilton's principle. Navier's analytical techniques are applied to obtain closed-form solutions for simply supported plates. A comprehensive parametric study is conducted, analyzing the impact of factors such as glass powder volume, geometric parameters, and thermal loading on the thermomechanical behavior of the panel. The findings highlight the challenges associated with using glass powder in concrete for thermomechanical applications and suggest the need for alternative approaches to optimize its effectiveness in such scenarios, also the study provides first-time numerical results that serve as guidelines for further research on reinforced concrete.

Keywords

thermomechanical behavior, reinforced concrete, plate theory, glass powder, homogenization

1 Introduction

The design and responsible maintenance of a healthy built environment taking into account resource efficiency and ecological is known as sustainable construction practice [1]. Concrete has become a popular construction material worldwide due to its versatility and affordability, yet also has effects on the environment [2]. A significant source of greenhouse gas emissions is the production of cement, a necessary component for the creation of concrete [3]. Using supplemental cementitious materials (SCMs) to replace some of the cement in concrete is a viable strategy for lowering the industry's environmental effect. Glass powder reinforced concrete is a type of concrete that is made by adding glass powder to the mixture. This type of concrete has several advantages over traditional concrete, including increased strength and durability. The glass powder used in this type of concrete is usually made from recycled glass, which makes it an eco-friendly option for

construction projects. Additionally, the use of glass powder in the mixture can reduce the amount of cement needed, which can help to lower costs.

One of the main properties of glass powder reinforced concrete is its high compressive strength. This makes it ideal for use in construction projects that require strong, durable materials, such as bridges and buildings. In addition, this type of concrete also has good thermal isolation properties, which can help to reduce energy costs in buildings. It is also resistant to chemical corrosion, making it a good choice for structures that will be exposed to harsh chemicals or saltwater environments.

Glass powder reinforced concrete (GPRC) is a composite material that consists of cement, water, fine and coarse aggregates, and glass powder. Experimentations on the use of glass powder as a partial replacement for cement in concrete has been gaining popularity due to its numerous

benefits. Ghareeb et al. [4] used recycled glass (GP) and lime powder (LP) as substitution materials in the manufacture of the UHPSCC. The tensile, flexural, and compressive strength were all increased by using GP up to 20% replacement of cement. Sadiquul Islam et al. [5] carried out compressive tests on concrete cube samples that had been manufactured until 1-year curing. The findings of the compressive strength test showed that concrete and mortar made from recycled glass were stronger than the control samples. At 20% replacement of cement with waste glass was found convincing considering cost and the environment. Paul et al. [6] used waste glass as a replacement for cement in concrete. The results show that concrete with 30% partial cement replacement by GP is a potential option for the construction industry while providing a management waste solution. Hamoudeh et al. [7] examined the impact of recycled crushed glass, both fine and coarse, on the density and flexural strength of concrete. Their results demonstrate that recovered glass waste can produce concrete that is both affordable and environmentally benign by replacing natural aggregate. Asgarian et al. [8] exhibited two grades of WGP: fine glass powder (FGP) and ultrafine glass powder (UFG) as cement substitutes, respectively, at 5% and 10% of the cement content in concrete reinforced with polypropylene (PP) fiber. The highest mechanical performance is achieved by 10% UFG as cement replacement and 0.5% PP fiber inclusion.

Mathematically speaking, there is a dearth of studies in the literature investigating the effect of glass powder on reinforced concrete. Ming et al. [9] established a theoretical model of the binary hydraulic kinetics model of glass powder-cement to investigate the effect of glass powder on cement hydration. The research revealed the hydration mechanism of glass powder and provided a theoretical basis for the application of glass powder in concrete. Raydan et al. [10] investigated the effect of utilizing glass powder in concrete as partial replacement for Portland cement and serve in developing numerical equations. Several equations have been developed to show a relation between the strength expected in terms of an average increasing or decreasing ratio and the percentage of replacement of cement with waste glass powder. Golafshani and Khashani [11] gathered from multiple peer-reviewed papers [12–17] on comprehensive database of concrete containing WG (CCWG) and used a novel machine learning method, called multi-objective multi-biogeography-based programming to predict the compressive strength of concrete containing waste glass.

The findings demonstrate that the suggested approach is capable of introducing a number of equations with various degrees of accuracy, complexity, and input variables to forecast the compressive strength of CCWG.

To the best of the author's knowledge, and motivated by the considerations that the effect of using glass powder on the thermomechanical analysis of concrete slabs has not been investigated before, we aim to present a mathematical model for simulating the equivalent system. The reinforced eco-concrete properties are considered based on Eshelby's approach. Herein, the glass powder employed in this research is referred to as glass nanoparticles, and the structure is simulated with higher order shear deformation theory model. The governing equations are obtained based on the principle of virtual work, and using Navier's analytical solutions, the effects of different parameters such as volume percent of glass powder, thermal loading type, and geometrical parameters, on the thermomechanical analysis of the panel are calculated and shown.

The findings of this study will contribute to a better understanding of the thermomechanical response of glass powder-based concrete panels, thereby aiding in the development of guidelines for their practical applications. Additionally, the study will shed light on the limitations and challenges associated with using glass powder in concrete for thermomechanical purposes, providing valuable insights for future research and development efforts.

2 Micromechanical model

The Eshelby Model is a mathematical model used to describe the homogenization of materials. It is based on the theory of elasticity and is used to predict the behavior of materials when subjected to different stresses and strains. The model was developed by the British physicist John Eshelby in the 1950s [18]. The model consists of three components: the strain field, the stress field, and the elastic modulus. The strain field is a mathematical description of the deformation of a material when it is subjected to a given load. The stress field is a mathematical description of the forces acting on the material. The elastic modulus is a measure of the material's stiffness.

The Eshelby Model accurately predicts stress and strain fields, enabling the behavior prediction of materials in various loading conditions like fatigue tests or thermal/mechanical stress. It also aids in designing robust components to withstand extreme loads.

The most significant analytical model for predicting the characteristics of a nano-composite reinforced matrix

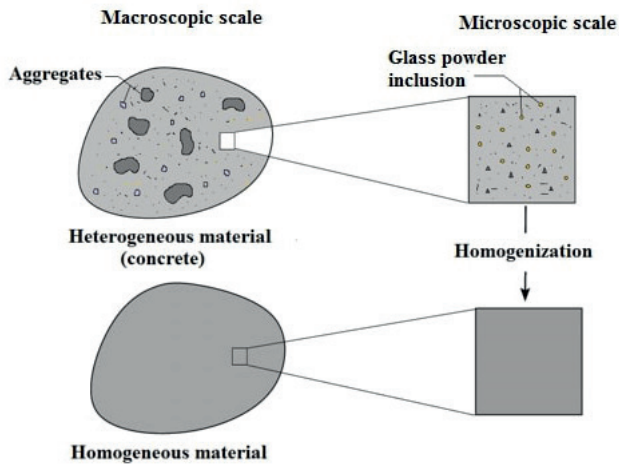


Fig. 1 Homogenization of concrete reinforced with glass powder inclusions

is Eshelby's homogenization model. Since it actually only applies to the placement of an ellipsoidal inclusion in an infinite matrix. The glass powder employed in this research as shown in Fig. 1 is referred to as glass nanoparticles due to its fine particle size and nanoscale dimensions. The nano composite's stiffness tensor C_T is given by:

$$C_T = \left(C_m^{-1} - V_r \{ (C_r - C_m) [S - V_r (S - I)] + C_m \}^{-1} (C_r - C_m) C_m^{-1} \right)^{-1} \quad (1)$$

In which, I is the identity matrix, C_m and C_r are the stiffness tensors for the concrete matrix and the glass powder reinforcement, respectively. While V_m and V_r are the volume fraction of the matrix and reinforcement, and S is the Eshelby's tensor which is related to the Poisson ratios of reinforcement.

For both isotropic materials the stiffnesses C_m and C_r are expressed as:

$$\begin{aligned} C_{11} = C_{22} &= \frac{(1-\nu)E}{(1+\nu)(1-2\nu)}, \\ C_{12} &= \frac{\nu E}{(1+\nu)(1-2\nu)}, \\ C_{44} = C_{55} = C_{66} &= \frac{E}{(1+\nu)}. \end{aligned} \quad (2)$$

In which E is the young's modulus of either the concrete matrix or the glass powder reinforcement, and ν are Poisson's ratios. The indexes 1, 2, 3 conform to x, y, z directions of the composite Cartesian coordinate system, respectively. For reinforcement with spherical form as depicted in Fig. 2, S is given as [19]:

$$S = \begin{bmatrix} S_{1111} & S_{1122} & S_{1133} & S_{1123} & S_{1113} & S_{1112} \\ S_{2211} & S_{2222} & S_{2233} & S_{2223} & S_{2213} & S_{2212} \\ S_{3311} & S_{3322} & S_{3333} & S_{3323} & S_{3313} & S_{3312} \\ S_{2311} & S_{2322} & S_{2333} & S_{2323} & S_{2313} & S_{2312} \\ S_{1311} & S_{1322} & S_{1333} & S_{1323} & S_{1313} & S_{1312} \\ S_{1211} & S_{1222} & S_{1233} & S_{1123} & S_{1213} & S_{1212} \end{bmatrix} \quad (3)$$

where:

$$\begin{aligned} S_{1111} = S_{2222} = S_{3333} &= \frac{7 - 5\nu_r}{15(1 - \nu_r)}, \\ S_{1122} = S_{1133} = S_{2233} = S_{2211} = S_{3311} = S_{3322} &= \frac{-1 + 5\nu_r}{15(1 - \nu_r)}, \\ S_{1212} = S_{1313} = S_{2323} &= \frac{4 - 5\nu_r}{15(1 - \nu_r)}. \end{aligned} \quad (4)$$

Here, ν_r denotes the Poisson's ratio of glass powder.

For particulate composites, the Eshelby's approach for the prediction of the thermal expansion α_T is presented in the form:

$$\alpha_T = \alpha_m - V_r \{ (C_m - C_r) [S - V_r (S - I)] - C_m \}^{-1} C_r (\alpha_r - \alpha_m) \quad (5)$$

Here, α_r and α_m are the reinforcement and matrix expansion tensors, respectively. C_m and C_r are the same stiffness tensors, but S tensor is now appropriate for heat properties, in which:

$$S_{11} = S_{22} = S_{33} = \frac{1}{3}. \quad (6)$$

For all others:

$$S_{ij} = 0. \quad (7)$$

Eshelby's homogenization theory can be applied over a wide temperature range, as it primarily focuses on the mechanical behavior (Elastic constant's) of materials and the redistribution of stresses and strains within a composite system. The theory is not inherently limited to a specific temperature range [18].

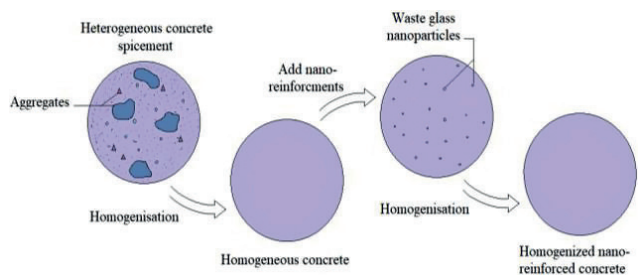


Fig. 2 Steps Homogenization of concrete reinforced with glass powder inclusions

3 Mathematical modeling of the panel

The study examines a flat concrete panel that is simply supported, with a length of L , width of b , and total thickness of h . As shown in Fig. 3, the reinforcement of the slab involves waste glass particles that are dispersed randomly at a nanoscale level within the concrete matrix.

Additionally, the selected coordinate system (x , y , and z) is shown in Fig. 3, in which:

$$0 \leq x \leq L; 0 \leq y \leq b; -h/2 \leq z \leq h/2. \quad (8)$$

To ensure precise numerical analysis, we employed various plate theories, specifically, higher-order shear deformation theories (HSDTs) known for their demonstrated effectiveness in accurately analyzing panel behavior under thermal load. By utilizing HSDTs, a valuable tool for our study, we ensured comprehensive analysis and precise results.

The displacement field of a material point positioned at (x , y , z) within the panel under the HSDT can be expressed in the following manner:

$$\begin{aligned} U(x, y, z) &= u_0(x, y) - z \frac{dw_0(x, y)}{dx} + f(z)\theta_x, \\ V(x, y, z) &= v_0(x, y) - z \frac{dw_0(x, y)}{dy} + f(z)\theta_y, \end{aligned} \quad (9)$$

$$W(x, y, z) = w_0(x, y).$$

The displacements in the x , y , and z directions are represented by U , V , and W , respectively. The mid-plane translations are denoted by u_0 , v_0 , and w_0 , while the rotations of the normal to the mid-plane around the y -axis and x -axis are indicated by θ_y and θ_x , respectively. The distribution of transverse shear strain and stress through the thickness is determined by the shape function, $f(z)$.

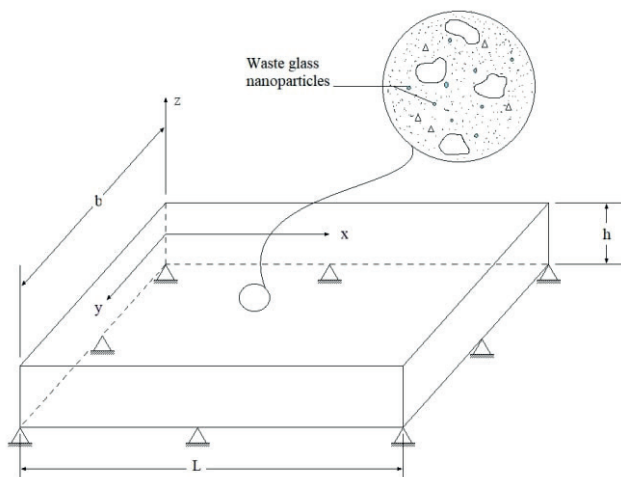


Fig. 3 Geometry and coordinate of a simply supported glass powder-reinforced concrete panel

By setting the displacement of the parabolic shear deformation plate theory (PSDPT), the formula is obtained as per [20]:

$$f(z) = z \left(1 - \frac{4z^2}{3h^2} \right). \quad (10)$$

The trigonometric shear deformation plate theory (SSDPT) can also be derived by setting the following equation, according to Touratier et al. [21]:

$$f(z) = \frac{h}{\pi} \sin \left(\frac{\pi z}{h} \right). \quad (11)$$

Furthermore, the displacement of the exponential shear deformation plate theory (ESDPT) can be obtained by applying the equation suggested by Karama et al. [22]:

$$f(z) = z e^{-2(z/h)^2}. \quad (12)$$

3.1 Refined trigonometric shear deformation theory

To further our analysis, we utilized a refined displacement field based on Huu Thai Tai's hypotheses [23]. The displacement field for the refined trigonometric theory can be expressed as follows:

$$\begin{aligned} U(x, y, z) &= u_0(x, y) - z \frac{dw_b(x, y)}{dx} - f(z) \frac{dw_s(x, y)}{dx}, \\ V(x, y, z) &= v_0(x, y) - z \frac{dw_b(x, y)}{dy} - f(z) \frac{dw_s(x, y)}{dy}, \\ W(x, y, z) &= w_b(x, y) + w_s(x, y). \end{aligned} \quad (13)$$

Where, u_0 and v_0 are the mid-plane displacements of the panel along the x and y direction. w_b and w_s are the bending and shear components of transverse displacement in z direction, respectively.

We utilized the trigonometric shape function $f(z)$ to express the transverse shear distribution through the panel thickness:

$$f(z) = z - \left(\frac{h}{\pi} \right) \sin \left(\frac{\pi z}{h} \right). \quad (14)$$

Unlike the first-order shear deformation theory, it is worth noting that refined plate theories do not necessitate the use of shear correction factors.

The displacement field in Eq. (13) can be used to calculate the components of linear strains.

$$\begin{aligned}
 \varepsilon_x &= \varepsilon_x^0 - zk_x^b - f(z)k_x^s, \\
 \gamma_{xy} &= \gamma_{xy}^0 - z\gamma_{xy}^b - f(z)\gamma_{xy}^s, \\
 \varepsilon_y &= \varepsilon_y^0 - zk_y^b - f(z)k_y^s, \\
 \gamma_{yz} &= \left(1 - \frac{df(z)}{dz}\right)\gamma_{yz}^s = g(z)\gamma_{yz}^s, \\
 \varepsilon_z &= 0, \\
 \gamma_{xz} &= \left(1 - \frac{df(z)}{dz}\right)\gamma_{xz}^s = g(z)\gamma_{xz}^s,
 \end{aligned} \tag{15}$$

where:

$$\begin{aligned}
 \varepsilon_x^0 &= \frac{du_0}{dx}; k_x^b = \frac{dw_b}{dx}; k_x^s = \frac{dw_s}{dx}; \varepsilon_y^0 = \frac{dv_0}{dy}, \\
 k_x^b &= \frac{dw_b}{dy}; k_x^s = \frac{dw_s}{dy}; \gamma_{xy}^0 = \frac{dv_0}{dx} + \frac{du_0}{dy}, \\
 k_x^b &= -2\frac{d^2w_b}{dxdy}; k_x^s = \frac{d^2w_s}{dxdy}; \gamma_{yz}^s = \frac{dw_s}{dy}; \gamma_{xz}^s = \frac{dw_s}{dx}, \\
 g(z) &= 1 - \frac{df(z)}{dz}.
 \end{aligned} \tag{16}$$

The constitutive stress-strain relations of the nano-composite concrete slab under thermo-elastic bending loads can be defined as:

$$\begin{Bmatrix} \sigma_x \\ \sigma_y \\ \tau_{xy} \\ \tau_{yz} \\ \tau_{xz} \end{Bmatrix} = \begin{bmatrix} C_T^{11} & C_T^{12} & 0 & 0 & 0 \\ C_T^{12} & C_T^{22} & 0 & 0 & 0 \\ 0 & 0 & C_T^{55} & 0 & 0 \\ 0 & 0 & 0 & C_T^{44} & 0 \\ 0 & 0 & 0 & 0 & C_T^{66} \end{bmatrix} \begin{Bmatrix} \varepsilon_x - \alpha T \\ \varepsilon_y - \alpha T \\ \gamma_{xy} \\ \gamma_{yz} \\ \gamma_{xz} \end{Bmatrix}, \tag{17}$$

where C_T^{ij} are the reduced elastic constants of the concrete panel reinforced with nano-sized glass powder, obtained using Eshelby's homogenization approach.

3.2 Principle of virtual work

The equations of motion are derived by employing the principle of virtual work:

$$\int_0^t (\delta\Psi) dt = 0, \tag{18}$$

where, $\delta\Psi$ is the virtual variation of the internal strain energy expressed as follows:

$$\delta\Psi = \int_{-h/2}^{h/2} \int_A (\sigma_x \delta\varepsilon_x + \sigma_y \delta\varepsilon_y + \tau_{xy} \delta\gamma_{xy} + \tau_{yz} \delta\gamma_{yz} + \tau_{xz} \delta\gamma_{xz}) dAdz \tag{19}$$

By substituting Eq. (15) into Eq. (19), one finds:

$$\delta\Psi = \int_A \left\{ \begin{aligned} &N_x \delta u_{0,x} - M_x^b \delta w_{b,x} + M_x^s \delta w_{s,x} \\ &+ N_y \delta v_{0,y} - M_y^b \delta w_{b,x} + M_y^s \delta w_{s,x} \\ &+ M_{xy}^b 2\delta w_{b,x,y} + N_{xy} (\delta u_{0,y} + \delta v_{0,x}) \\ &+ M_{xy}^s 2\delta w_{s,x,y} + Q_{yz} \delta w_{s,y} + Q_{xz} \delta w_{s,x} \end{aligned} \right\} dA \tag{20}$$

where, stress resultants can be expressed as follows:

$$\begin{aligned}
 (N_x, N_y, N_{xy}) &= \int_{-h/2}^{h/2} (\sigma_x, \sigma_y, \tau_{xy}), \\
 (M_x^b, M_y^b, M_{xy}^b) &= \int_{-h/2}^{h/2} z (\sigma_x, \sigma_y, \tau_{xy}), \\
 (M_x^s, M_y^s, M_{xy}^s) &= \int_{-h/2}^{h/2} f(z) (\sigma_x, \sigma_y, \tau_{xy}), \\
 (Q_{yz}, Q_{xz}) &= \int_{-h/2}^{h/2} g(z) (\sigma_{yz}, \sigma_{xz}).
 \end{aligned} \tag{21}$$

The equilibrium equations associated with the trigonometric refined shear deformation theory can be derived from Eq. (20) by integrating parts and collecting the coefficients of δu_0 , δv_0 , δw_b and δw_s :

$$\begin{aligned}
 \delta u_0: \frac{dN_x}{dx} + \frac{dN_{xy}}{dy} &= 0, \\
 \delta v_0: \frac{dN_y}{dy} + \frac{dN_{xy}}{dx} &= 0, \\
 \delta w_b: \frac{d^2 M_x^b}{dx^2} + \frac{d^2 M_{xy}^b}{dxdy} + \frac{d^2 M_x^b}{dy^2} &= 0, \\
 \delta w_s: \frac{d^2 M_x^s}{dx^2} + \frac{d^2 M_{xy}^s}{dxdy} + \frac{d^2 M_x^s}{dy^2} + \frac{dQ_{yz}}{dy} + \frac{dQ_{xz}}{dx} &= 0.
 \end{aligned} \tag{22}$$

By substituting Eq. (17) into Eq. (21), one obtains the stress resultants in form of material stiffness and displacement components:

$$\begin{aligned}
 \begin{Bmatrix} N_x \\ N_y \\ N_{xy} \end{Bmatrix} &= \begin{bmatrix} A_{11} & A_{12} & 0 \\ A_{12} & A_{22} & 0 \\ 0 & 0 & A_{66} \end{bmatrix} \begin{Bmatrix} \frac{du_0}{dx} \\ \frac{dv_0}{dy} \\ \frac{du_0}{dy} + \frac{dv_0}{dx} \end{Bmatrix} + \begin{bmatrix} B_{11} & B_{12} & 0 \\ B_{12} & B_{22} & 0 \\ 0 & 0 & B_{66} \end{bmatrix} \begin{Bmatrix} \frac{d^2w_b}{dx^2} \\ \frac{d^2w_b}{dy^2} \\ -2\frac{d^2w_b}{dxdy} \end{Bmatrix} + \begin{bmatrix} Bs_{11} & Bs_{12} & 0 \\ Bs_{12} & Bs_{22} & 0 \\ 0 & 0 & Bs_{66} \end{bmatrix} \begin{Bmatrix} \frac{d^2w_s}{dx^2} \\ \frac{d^2w_s}{dy^2} \\ -2\frac{d^2w_s}{dxdy} \end{Bmatrix} - \begin{Bmatrix} N_T^x \\ N_T^y \\ N_T^{xy} \end{Bmatrix} \\
 \begin{Bmatrix} M_x^b \\ M_y^b \\ M_{xy}^b \end{Bmatrix} &= \begin{bmatrix} B_{11} & B_{12} & 0 \\ B_{12} & B_{22} & 0 \\ 0 & 0 & B_{66} \end{bmatrix} \begin{Bmatrix} \frac{du_0}{dx} \\ \frac{dv_0}{dy} \\ \frac{du_0}{dy} + \frac{dv_0}{dx} \end{Bmatrix} + \begin{bmatrix} D_{11} & D_{12} & 0 \\ D_{12} & D_{22} & 0 \\ 0 & 0 & D_{66} \end{bmatrix} \begin{Bmatrix} \frac{d^2w_b}{dx^2} \\ \frac{d^2w_b}{dy^2} \\ -2\frac{d^2w_b}{dxdy} \end{Bmatrix} + \begin{bmatrix} Ds_{11} & Ds_{12} & 0 \\ Ds_{12} & Ds_{22} & 0 \\ 0 & 0 & Ds_{66} \end{bmatrix} \begin{Bmatrix} \frac{d^2w_s}{dx^2} \\ \frac{d^2w_s}{dy^2} \\ -2\frac{d^2w_s}{dxdy} \end{Bmatrix} - \begin{Bmatrix} M_{bT}^x \\ M_{bT}^y \\ M_{bT}^{xy} \end{Bmatrix} \\
 \begin{Bmatrix} M_x^s \\ M_y^s \\ M_{xy}^s \end{Bmatrix} &= \begin{bmatrix} B_{11} & B_{12} & 0 \\ B_{12} & B_{22} & 0 \\ 0 & 0 & B_{66} \end{bmatrix} \begin{Bmatrix} \frac{du_0}{dx} \\ \frac{dv_0}{dy} \\ \frac{du_0}{dy} + \frac{dv_0}{dx} \end{Bmatrix} + \begin{bmatrix} D_{11} & D_{12} & 0 \\ D_{12} & D_{22} & 0 \\ 0 & 0 & D_{66} \end{bmatrix} \begin{Bmatrix} \frac{d^2w_b}{dx^2} \\ \frac{d^2w_b}{dy^2} \\ -2\frac{d^2w_b}{dxdy} \end{Bmatrix} + \begin{bmatrix} Ds_{11} & Ds_{12} & 0 \\ Ds_{12} & Ds_{22} & 0 \\ 0 & 0 & Ds_{66} \end{bmatrix} \begin{Bmatrix} \frac{d^2w_s}{dx^2} \\ \frac{d^2w_s}{dy^2} \\ -2\frac{d^2w_s}{dxdy} \end{Bmatrix} - \begin{Bmatrix} M_{sT}^x \\ M_{sT}^y \\ M_{sT}^{xy} \end{Bmatrix}
 \end{aligned} \tag{23}$$

Here, A_{ij} , B_{ij} , D_{ij} , Bs_{ij} , Ds_{ij} , HS_{ij} , and As_{ij} are the plate stiffness constants, defined by:

$$\begin{aligned}
 [A_{ij}, B_{ij}, D_{ij}] &= \int_{h_n}^{h_{n+1}} C_T^{ij} [1, z, z^2] dz \\
 [Bs_{ij}, Ds_{ij}, HS_{ij}] &= \int_{h_n}^{h_{n+1}} C_T^{ij} [f(z), zf(z), f(z)^2] dz \\
 [As_{ij}] &= \int_{h_n}^{h_{n+1}} C_T^{ij} [g(z)^2] dz
 \end{aligned} \tag{24}$$

The normal stress and moment resultants $N_x^T = N_y^T$, $M_{bT}^x = M_{bT}^y$ and $M_{sT}^x = M_{sT}^y$ caused by the external thermal loading are defined by:

$$\begin{Bmatrix} N_T^x \\ M_{bT}^x \\ M_{sT}^x \end{Bmatrix} = \int_{-h/2}^{h/2} C_T^{11} \alpha_T T \begin{Bmatrix} 1 \\ z \\ f(z) \end{Bmatrix} dz. \tag{25}$$

It is assumed that the variation of the temperature field through the thickness is expressed as:

$$T(x, y, z) = T_1(x, y) + \frac{z}{h} T_2(x, y) + \frac{\psi(z)}{h} T_3(x, y). \tag{26}$$

Here T_1 , T_2 and T_3 are thermal loadings, and for the case of the present refined trigonometric theory (RTSDT):

$$\psi(z) = \frac{h}{\pi} \sin\left(\frac{\pi z}{h}\right). \tag{27}$$

Substituting from Eq. (23) into Eq. (22) one finds:

$$\begin{aligned}
 A_{11}d_{11}u_0 + A_{66}d_{22}u_0 + (A_{12} + A_{66})d_{12}v_0 - B_{11}d_{111}w_b - (B_{12} + 2B_{66})d_{122}w_b - (B_{s12} + 2B_{s66})d_{122}w_s - B_{s11}d_{111}w_s &= f_1 \\
 A_{22}d_{22}v_0 + A_{66}d_{22}v_0 + (A_{12} + A_{66})d_{12}u_0 - B_{22}d_{222}w_b - (B_{12} + 2B_{66})d_{112}w_b - (B_{s12} + 2B_{s66})d_{112}w_s - B_{s22}d_{222}w_s &= f_2 \\
 B_{11}d_{111}u_0 + (B_{12} + B_{66})d_{122}u_0 + (B_{12} + B_{66})d_{112}v_0 + B_{22}d_{222}v_0 - D_{11}d_{1111}w_b - 2(D_{12} + 2D_{66})d_{1122}w_b - D_{22}d_{2222}w_b \\
 - D_{s11}d_{1111}w_s - 2(D_{s12} + 2D_{s66})d_{1122}w_s - D_{s22}d_{2222}w_s &= f_3 \\
 B_{s11}d_{111}u_0 + (B_{s12} + B_{s66})d_{122}u_0 + (B_{s12} + B_{s66})d_{112}v_0 + B_{s22}d_{222}v_0 - D_{s11}d_{1111}w_b - 2(D_{s12} + 2D_{s66})d_{1122}w_b - D_{s22}d_{2222}w_b \\
 - D_{s11}d_{1111}w_s - 2(H_{s12} + 2H_{s66})d_{1122}w_s - H_{s22}d_{2222}w_s - A_{s55}d_{11}w_s - A_{s44}d_{22}w_s &= f_4
 \end{aligned} \tag{28}$$

The generalized force vector is described as $\{f\} = \{f_1, f_2, f_3, f_4\}^T$, while, d_i, d_{ij}, d_{ijl} and d_{ijlm} are differential operators expressed as the following:

$$\begin{aligned}
 d_i &= \frac{\partial}{\partial x_i}, \\
 d_{ij} &= \frac{\partial^2}{\partial x_i \partial x_j}, \\
 d_{ijl} &= \frac{\partial^3}{\partial x_i \partial x_j \partial x_l}, \\
 d_{ijlm} &= \frac{\partial^4}{\partial x_i \partial x_j \partial x_l \partial x_m}, \quad (i, j, l, m = 1, 2).
 \end{aligned}
 \tag{29}$$

The components of the generalized force vector $\{f\}$ are:

$$\begin{aligned}
 f_1 &= \frac{\partial N_T^x}{\partial x}, \\
 f_2 &= \frac{\partial N_T^y}{\partial y}, \\
 f_3 &= -\frac{\partial^2 M_{bT}^x}{\partial x^2} - \frac{\partial^2 M_{bT}^y}{\partial y^2}, \\
 f_4 &= -\frac{\partial^2 M_{sT}^x}{\partial x^2} - \frac{\partial^2 M_{sT}^y}{\partial y^2}.
 \end{aligned}
 \tag{30}$$

3.3 Navier's technique

To formulate the closed-form solutions for bending problems of simply supported rectangular plate for the refined trigonometric shear deformation theory, Navier's method is employed:

$$\begin{aligned}
 u_0(x, y, t) &= \sum_{m=1}^{\infty} \sum_{n=1}^{\infty} U_{mn} \cos(\lambda x) \sin(\varphi y), \\
 v_0(x, y, t) &= \sum_{m=1}^{\infty} \sum_{n=1}^{\infty} V_{mn} \sin(\lambda x) \cos(\varphi y), \\
 w_b(x, y, t) &= \sum_{m=1}^{\infty} \sum_{n=1}^{\infty} W_{bmn} \sin(\lambda x) \sin(\varphi y), \\
 w_s(x, y, t) &= \sum_{m=1}^{\infty} \sum_{n=1}^{\infty} W_{smn} \sin(\lambda x) \sin(\varphi y).
 \end{aligned}
 \tag{31}$$

Where, U_{mn}, V_{mn}, W_{bmn} and W_{smn} are the arbitrary parameters to be determined, $\lambda = m\pi/a, \varphi = n\pi/b$.

The closed-form solutions are checked for:

$$\begin{aligned}
 u_0(x, 0) = w_b(x, 0) = w_s(x, 0) &= \frac{dw_b}{dx}(x, 0) = \frac{dw_s}{dx}(x, 0) = 0, \\
 u_0(x, b) = w_b(x, b) = w_s(x, b) &= \frac{dw_b}{dx}(x, b) = \frac{dw_s}{dx}(x, b) = 0, \\
 u_0(0, y) = w_b(0, y) = w_s(0, y) &= \frac{dw_b}{dx}(0, y) = \frac{dw_s}{dx}(0, y) = 0, \\
 u_0(x, b) = w_b(a, y) = w_s(a, y) &= \frac{dw_b}{dx}(a, y) = \frac{dw_s}{dx}(a, y) = 0.
 \end{aligned}
 \tag{32}$$

For boundary conditions other than simply supported, it is necessary to adopt a different type of solution that can adequately satisfy those specific boundary conditions.

Navier presented the transverse temperature loads T_1, T_2 , and T_3 in the form of a double trigonometric series as:

$$\begin{Bmatrix} T_1 \\ T_2 \\ T_3 \end{Bmatrix} = \begin{Bmatrix} \bar{T}_1 \\ \bar{T}_2 \\ \bar{T}_3 \end{Bmatrix} \sin(\lambda x) \sin(\varphi y) \times \begin{cases} 1 & \text{for sinusoidal load} \\ (m = n = 1) \\ \frac{16}{mn\pi^2} & \text{for uniform load} \\ (m = n = 1, 3, 5, \dots) \end{cases}
 \tag{33}$$

Substituting Eq. (31) into Eq. (22), one obtains the closed-form solutions in matrix form:

$$[K_{ij}] \{\Delta\} = \{f\},
 \tag{34}$$

where:

$$\{\Delta\} = \{U_{mn}, V_{mn}, W_{bmn}, W_{smn}\}^T.
 \tag{35}$$

The components of the elastic stiffness matrix $[K_{ij}]$ are as follows:

$$[K_{ij}] = \begin{bmatrix} k_{11} & k_{12} & k_{13} & k_{14} \\ k_{21} & k_{22} & k_{23} & k_{24} \\ k_{31} & k_{32} & k_{33} & k_{34} \\ k_{41} & k_{42} & k_{43} & k_{44} \end{bmatrix},
 \tag{36}$$

where:

$$\begin{aligned}
 k_{11} &= -A_{11}\alpha^2 - A_{66}\varphi^2 \\
 k_{22} &= -\alpha\varphi(A_{11} + A_{66}) \\
 k_{22} &= -A_{66}\alpha^2 - A_{22}\varphi^2 \\
 k_{13} &= B_{11}\alpha^3 + B_{12}\alpha\varphi^2 + 2B_{66}\alpha\varphi^2 \\
 k_{23} &= B_{11}\alpha^3 + B_{12}\varphi\alpha^2 + 2B_{66}\varphi\alpha^2 \\
 k_{14} &= Bs_{11}\alpha^3 + Bs_{12}\alpha\varphi^2 + 2Bs_{66}\alpha\varphi^2 \\
 k_{24} &= Bs_{11}\alpha^3 + Bs_{12}\varphi\alpha^2 + 2Bs_{66}\varphi\alpha^2 \\
 k_{31} &= k_{13}; k_{32} = k_{23} \\
 k_{33} &= -D_{11}\alpha^4 - 2\alpha^2\varphi^2(D_{12} + 2D_{66}) - D_{22}\varphi^4 \\
 k_{34} &= -Ds_{11}\alpha^4 - 2\alpha^2\varphi^2(Ds_{12} + 2Ds_{66}) - Ds_{22}\varphi^4 \\
 k_{41} &= k_{14} \\
 k_{42} &= k_{24} \\
 k_{43} &= k_{34} \\
 k_{44} &= -Hs_{11}\alpha^4 - 2\alpha^2\varphi^2(D_{12} + 2D_{66}) \\
 &\quad - Ds_{22}\varphi^4 - As_{44}\alpha^2 - As_{55}\alpha^2
 \end{aligned} \tag{37}$$

The components of the generalized force vector $\{f\} = \{f1, f2, f3, f4\}^T$, are given by:

$$\begin{aligned}
 f_1 &= \lambda(A_T \bar{T}_1 + B_T \bar{T}_2 + B_T^a \bar{T}_3), \\
 f_2 &= \varphi(A_T \bar{T}_1 + B_T \bar{T}_2 + B_T^a \bar{T}_3), \\
 f_3 &= -h(\lambda^2 + \varphi^2)(B_T \bar{T}_1 + D_T \bar{T}_2 + D_T^a \bar{T}_3), \\
 f_4 &= -h(\lambda^2 + \varphi^2)(B_T^s \bar{T}_1 + D_T^s \bar{T}_2 + F_T^s \bar{T}_3),
 \end{aligned} \tag{38}$$

where:

$$\begin{aligned}
 [A_T, B_T, D_T] &= \int_{-h/2}^{h/2} C_T^{11} (1 + \nu_T) \alpha_T [1, \bar{z}, \bar{z}^2] dz, \\
 [B_T^a, D_T^a] &= \int_{-h/2}^{h/2} C_T^{11} (1 + \nu_T) \alpha_T \bar{\psi}(z) [1, \bar{z}] dz, \\
 [B_T^s, D_T^s, F_T^s] &= \int_{-h/2}^{h/2} C_T^{11} (1 + \nu_T) \alpha_T \bar{f}(z) [1, \bar{z}, \bar{\psi}(z)] dz.
 \end{aligned} \tag{39}$$

In which:

$$\bar{z} = z / h, \quad \bar{f}(z) = f(z) / h, \quad \text{and} \quad \bar{\psi}(z) = \psi(z) / h. \tag{40}$$

4 Results and discussion

This section presents analytical results related to the thermo-elastic bending behavior of concrete panels reinforced with varying types and proportions of waste glass nano-powders. The refined sinusoidal plate deformation theory is utilized to calculate transverse displacements (w_T), axial stress ($\bar{\sigma}_x$), and shear stress ($\bar{\tau}_{xy}$). To demonstrate the thermal-structural analysis of a GP reinforced concrete slab, a range of sample problems are examined. Specifically, the linearly varying (across the thickness)

temperature distribution $T = \bar{z}T_2$, non-linearly varying (across the thickness) temperature distribution $T = \bar{\psi}(z)T_3$, and a combination of both $T = \bar{z}T_2 + \bar{\psi}(z)T_3$ are investigated. In this regard, various dimensionless quantities are employed for pure temperature loading, such as:

$$\begin{aligned}
 w_T &= \frac{h}{\alpha_0 T_2 a^2} w\left(\frac{a}{2}, \frac{b}{2}, 0\right), \\
 \bar{\sigma}_x(z) &= \frac{h^2}{\alpha_0 T_2 E_0 a^2} \sigma\left(\frac{a}{2}, \frac{b}{2}, z\right), \\
 \bar{\tau}_{xy}(z) &= \frac{10h}{\alpha_0 T_2 E_0 a} \tau\left(\frac{a}{2}, \frac{b}{2}, z\right).
 \end{aligned} \tag{41}$$

Herein, the reference values used are $E = 1$ GPa and $\alpha_0 = 10^{-6}/K$.

This work is highly relevant as it explores the use of various types of nanometric reinforcement in concrete matrices to evaluate and compare their mechanical and physical efficiency. By examining the performance of each nano-composite, this study provides valuable insights into the potential of these materials for enhancing the properties of concrete, which could have significant implications for the construction industry. In this analysis, nano-sized waste glass powders of different chemical composition and elastic characteristics are chosen to be explored as reinforcement in a concrete matrix. The thermo-elastic properties of these reinforcements such as, Young's modulus (E_p), Poisson's ration (ν_p), and thermal expansion (α_p) are given in Table 1.

The nano-sized glass powders are infused into a concrete mixture with an elastic modulus of $E_m = 20$ GPa, a Poisson's ratio of $\nu_m = 0.3$, and a thermal expansion of $\alpha_m = 13.5 \cdot 10^{-6}/K$ to create a nano-composite matrix. Eshelby's homogenization method is employed to forecast the elastic properties of the resultant nano-composite material.

4.1 Validation of the mathematical model

To begin, it is crucial to assess the accuracy of the current mathematical model, which is based on the refined sinusoidal plate theory assumptions. Since there is a lack of numerical results in the literature regarding the thermo-elastic

Table 1 Elastic characteristics of used glass powder

Code name for GP	Description	Young's modulus E_p (GPa)	Poisson's ration ν_p	Thermal expansion $\alpha_p (10^{-6}/K)$
Al-SiO ₂	Aluminosilicate glass powder	81	0.291	4.6
SiO ₂	Silicone glass powder	73	0.16	0.55

Table 2 Validation of the current theory with other theories in the literature, ($a/h = 10, a = b, \bar{T}_2 = 100, \bar{T}_3 = \bar{T}_1 = 0$)

Method	ω			σ_x			τ_{xz}		
	$p = 1$	$p = 2$	$p = 5$	$p = 1$	$p = 2$	$p = 5$	$p = 1$	$p = 2$	$p = 5$
Present	0.6063	0.6394	0.6659	2.1443	1.9822	1.8518	0.6949	0.6897	0.6693
Zenkour	0.6063	0.6394	0.6659	2.1444	1.9822	1.8519	0.6948	0.6896	0.6693
TSDT	0.6063	0.6393	0.6659	2.1444	1.9823	1.8519	0.5600	0.5568	0.5427
FSDT	0.6059	0.6390	0.6656	2.1447	1.9825	1.8521	/	/	/

flexural analysis of concrete panels reinforced with glass powder, we refer to the material and geometric properties used by Zenkour and Alghamdi [24] in their flexural analysis of sandwich plates made of functionally graded material (FGM). Table 2 presents the obtained results in terms of transverse displacements (ω), as well as normal and shear stresses (σ_x, τ_{xz}) of functionally graded (FG) beams, which are utilized for comparison purposes.

The comparison of the results displayed in Table 2 have been made for an FG beam subjected to uniformly distributed bending load, the results elucidate that the current results are in excellent agreement with those of Zenkour and Alghamdi [24]. Both refined sinusoidal and Zenkour's theories have predicted the same transverse displacement (ω) and shear stresses (σ_x, τ_{xz}) despite the different shape functions $f(z)$ used, thus the accuracy of the present adopted model is established. For the first-order beam theory (FSDT), the vertical displacement (ω) and shear stresses (σ_x, τ_{xz}) are slightly lower than those obtained by the refined sinusoidal plate theory, and this is mainly due to the fact that the FSDT plate theory doesn't take in to account the effect of shear stress across the thickness of the panel.

The data presented in Fig. 4 illustrates the effect of two different types of glass powder reinforcement, namely Al-SiO₂ and SiO₂ GP's, on the elastic stiffness (C_{ij}) of

a concrete matrix. It can be observed that both types of reinforcement have a positive impact on the elastic stiffness, as the concentration of reinforcements (V_r) increases. However, a more significant improvement in stiffness is evident in the case of Al-SiO₂ waste nano-glass powder, as depicted in Fig. 4. Specifically, in the (x, y) plane of the panel, the elastic stiffness C_{11} and C_{12} , denoting the elastic stiffness on the long-side x and xy directions, respectively, are noticeably improved with the addition of Al-SiO₂ GP. This enhancement can be attributed to the superior mechanical properties of the nanoparticle, including a high Young's modulus. Therefore, it can be noted that Al-SiO₂ GP is a more effective reinforcement material for improving the elastic stiffness of concrete matrices.

Additionally, the analysis depicted in Fig. 4 demonstrates that the optimal percentage share of nano-glass powder in concrete matrices is $V_r = 20$ wt%. This particular composition directly contributes to the enhanced characteristics of the plate, specifically in terms of its resistance against mechanical loads.

4.2 Thermo-elastic bending analysis

Fig. 5 presents a comparison of non-dimensional thermo-elastic transverse displacement (ω^T) values obtained using different plate theories, including sinusoidal refined

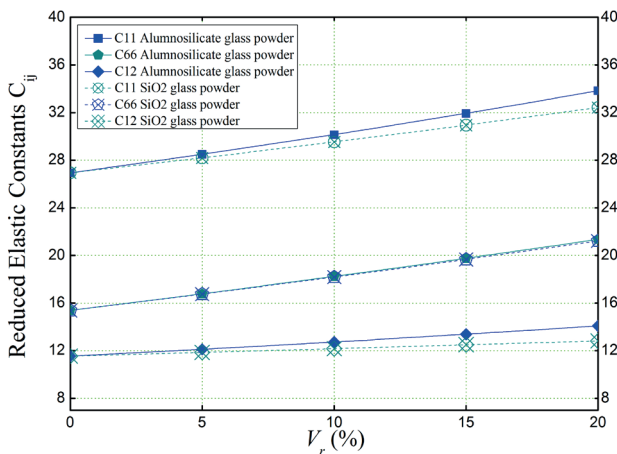


Fig. 4 Homogenized elastic stiffnesses C_{ij} of a concrete reinforced with glass powders

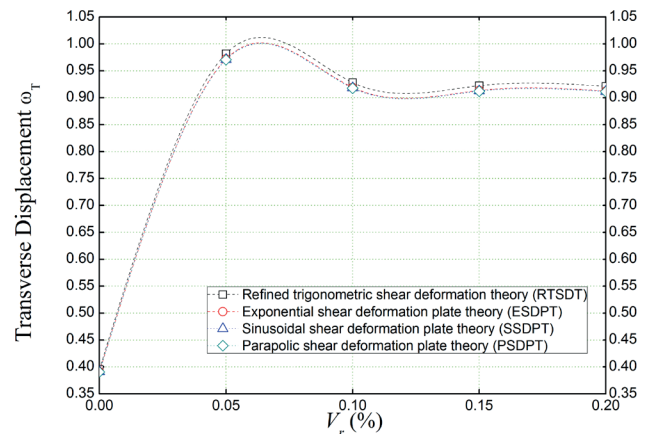


Fig. 5 Dimensionless center deflection of aluminosilicate glass powder reinforced concrete slab subjected to linearly varying thermal field ($a/h = 10, a = b, \bar{T}_2 = 100, \bar{T}_3 = \bar{T}_1 = 0$)

plate theory (SSDPT), exponential shear deformation theory (ESDPT), trigonometric shear deformation theory (TSDPT), and polynomial shear deformation theory (PSDPT), as a function of aluminosilicate glass powder reinforcement volumes in a concrete slab, the latter is considered subjected to a linearly varying across the thickness thermal load ($\bar{T}_2 = 100, \bar{T}_3 = \bar{T}_1 = 0$).

It is worth noting that all the theories show similar behavior, but the transverse deflection values predicted by the Refined Trigonometric Shear Deformation Theory (RTSDT) are slightly higher than the others. This is attributed to the shape function used to express the transverse shear stresses that evolve through the thickness of the plate. Despite this discrepancy, the sinusoidal refined plate theory appears to provide accurate results.

Furthermore, the graph shows that the incorporation of glass powder reinforcement in concrete slabs has a negative impact on their deflection. The deflection increases up to a maximum when 5% of Al-SiO₂ glass powder volume is added, after which it starts to stabilize as the reinforcement volume exceeds 10%.

Fig. 6 presents a comparison of non-dimensional thermo-elastic transverse displacement values obtained using the sinusoidal refined theory (RTSDT) as a function of reinforcement volumes (V_r). One curve shows the development of non-dimensional deflection (ω_T) for a concrete slab reinforced with aluminosilicate (Al-SiO₂) waste glass nano-sized powder, while the other curve shows the variation of (ω_T) for a concrete slab reinforced by silicate nano-glass powder. The elastic properties of these nano-composites are determined by Eshelby's homogenization law. It is assumed that the concrete panel is subjected to a non-linear varying load ($\bar{T}_2 = \bar{T}_3 = 100, \bar{T}_1 = 0$).

It can be observed from Fig. 6 that the use of Al-SiO₂ nanoparticles as reinforcement is more effective in increasing the deflection ω_T compared to silicate GP. This can be attributed to the high thermal expansion (α_T) and Young's elastic modulus, of the aluminosilicate GP, which leads to a higher deformation of the concrete nano-composite.

Fig. 7 presents the effect of geometric ratios (a/h , and a/b) on the non-dimensional transverse displacement (ω_T) of a simply supported concrete panel reinforced with various proportions of aluminosilicate nano-sized waste glass powder and exposed to different thermal loads. In Fig. 7(a), the effect of the length/thickness (a/h) ratio of a panel subjected to a linearly varying thermal load is shown with regard to different nanometric aluminosilicate GP incorporation volumes (V_r). Meanwhile, Fig. 7(b) shows the

effect of the length/width (a/b) ratio of a concrete panel subjected to a combination of linear and non-linear thermal field ($\bar{T}_2 = \bar{T}_3 = 100, \bar{T}_1 = 0$).

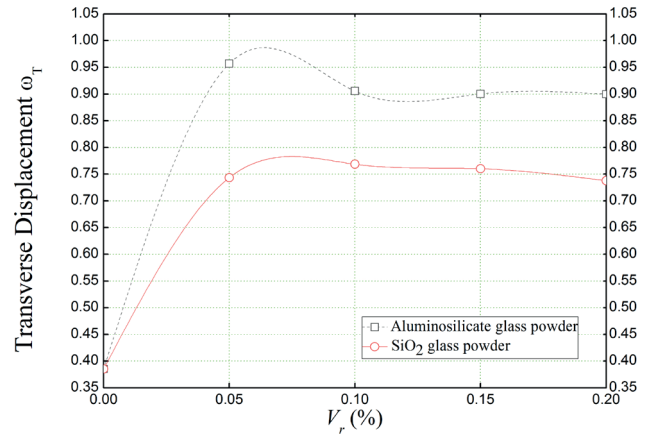


Fig. 6 Comparison between the effect of aluminosilicate and SiO₂ glass powders reinforcements on the non-dimensional transverse displacement of concrete slabs under non-linearly varying load ($a/h = 5, a = b, \bar{T}_2 = 100, \bar{T}_3 = \bar{T}_1 = 0$)

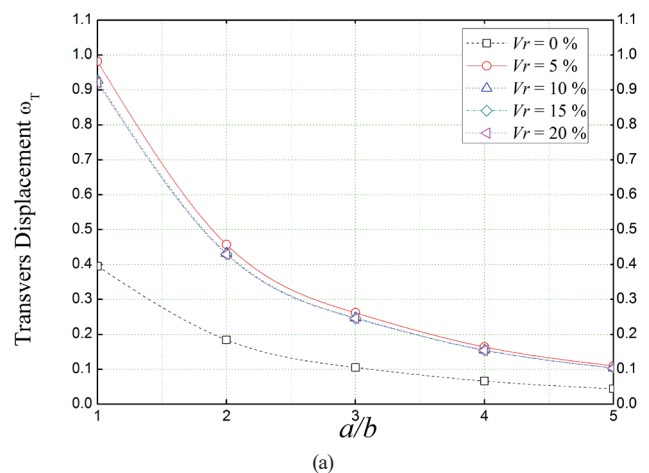
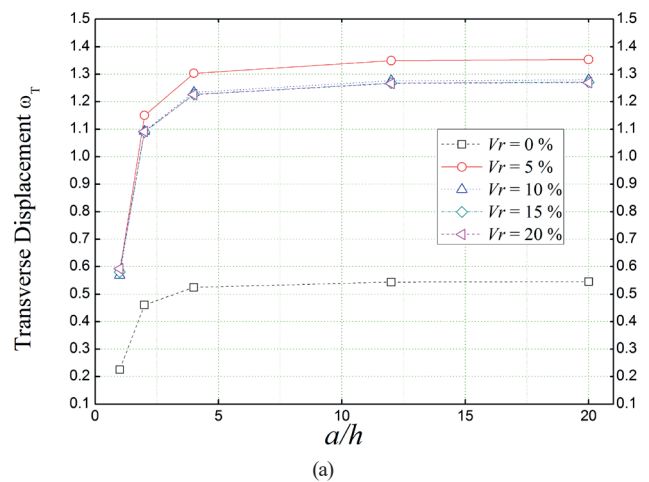


Fig. 7 Effect of geometric parameters on the non-dimensional center deflection of a GP reinforced concrete slab under different thermal loads; (a) $a = b, \bar{T}_2 = 100, \bar{T}_3 = \bar{T}_1 = 0$, (b) $a/h = 10, \bar{T}_2 = \bar{T}_3 = 100, \bar{T}_1 = 0$

These results further confirm the weakening effect of the nano glass powder on the panel, which is mainly due to the thermo-elastic properties of the incorporated nano-glass powder, such as high thermal expansion. Therefore, regardless of the geometric ratios, the higher the percentage of particles present in the concrete matrix, the higher the deflection becomes.

Fig. 8 presents the non-dimensional thermo-elastic deflection (ω_T) of a simply supported concrete panel subjected to a linearly varying thermal load ($\bar{T}_2 = 100$). The composite concrete beam is analytically modelled using several panel theories to predict the transverse displacement (ω_T) along the length (x/a). The composite panel is reinforced with either aluminosilicate (Al-SiO₂) or silicate (SiO₂) waste glass powder. In Fig. 8(a), the concrete panel is reinforced with a 5% proportion of glass powder, while in Fig. 8(b), the panel is reinforced with 20% of glass powder out of the total volume of the composite.

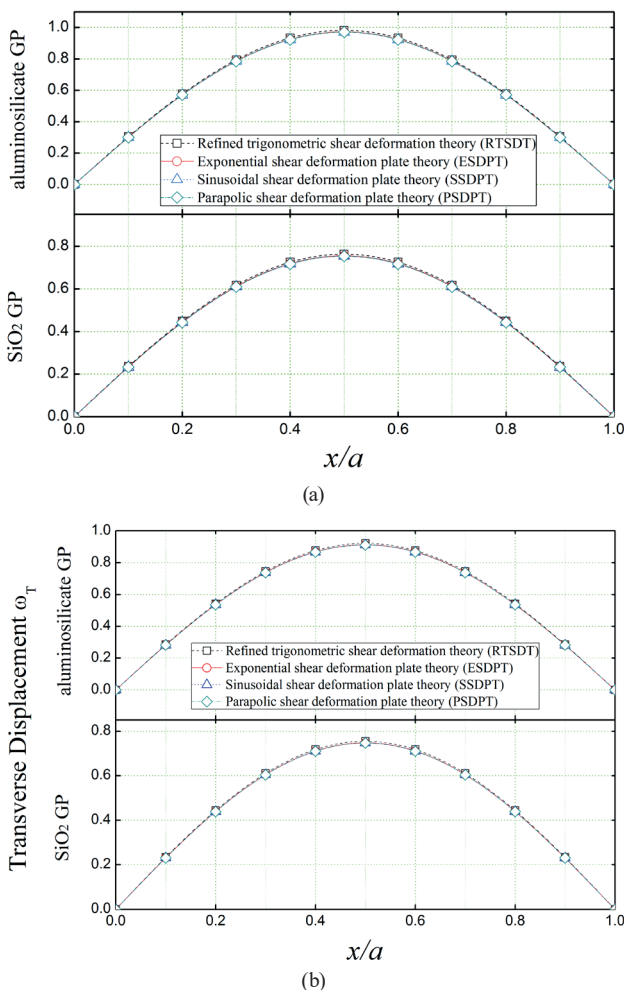


Fig. 8 Dimensionless transverse displacement of concrete slab reinforced with different glass powders ($a/h = 10$, $a = b$, $\bar{T}_2 = 100$, $\bar{T}_3 = \bar{T}_1 = 0$); (a) $V_r = 5\%$, (b) $V_r = 20\%$

Upon inspection of Fig. 8, it is evident that the deflection of the panel is slightly greater when the proportion of glass powder is 5% compared to when it is 20% reinforced.

Fig. 9 displays the effect of the length-to-thickness geometric ratio (L/h) on the non-dimensional thermo-elastic deflection (ω_T) of a concrete slab impregnated with aluminosilicate (Al-SiO₂) glass powder subjected to different linear and non-linear thermal loads. The results indicate that, regardless of the thermal loads, an increase in the length-to-thickness ratio of the panel leads to a higher deflection until the geometric ratio exceeds ($L/h > 20$), after which the deflection is stabilized. Furthermore, when the reinforced concrete panel is subjected to a non-linear thermal load $\bar{T}_3 = 100$, the deflection is minimal, and the panel is considered more resilient. On the other hand, when the panel is subjected to a load of $\bar{T}_3 = -100$, the deflection reaches its maximum value.

Fig. 10 illustrates the variation in the non-dimensional thermo-elastic transverse displacement (ω_T) of aluminosilicate glass powder reinforced concrete slab ($V_r = 15\%$) subjected to different linear and non-linear thermal loads as a function of the length-to-side geometric ratio (a/b). By highlighting the impact of (a/b) geometric ratio, the results indicate that the stability of the panel is lower when its geometry is rectangular ($a/b = 1$). Furthermore, Fig. 10 shows that the panel is more affected when exposed to a non-linear thermal load of $\bar{T}_3 = 100$, regardless of the length-to-thickness ratio (a/b).

Fig. 11 displays the plot of axial stress (σ_x) through the thickness (z/h) of a concrete slab, which is reinforced with aluminosilicate and silicon waste glass powder. The variation of the volume proportion of these reinforcements is taken into account by presenting the axial stress of a 5%

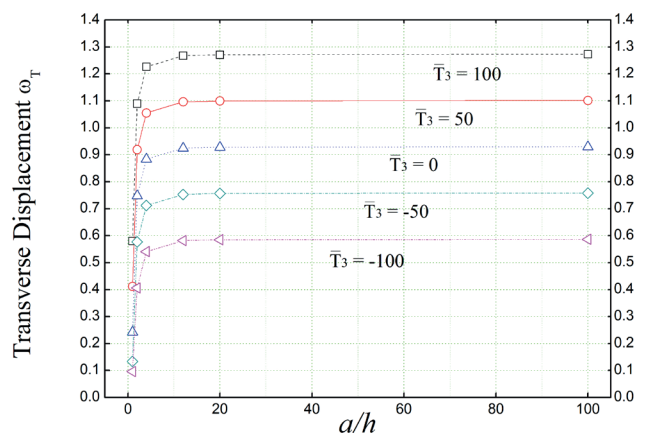


Fig. 9 Effect of length-to-thickness (a/h) ratio on the transverse displacement of a GP reinforced concrete slab under different thermal loads ($V_r = 15\%$, $a = b$)

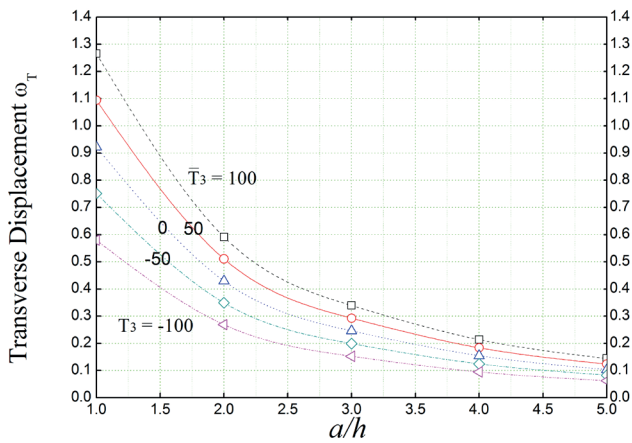


Fig. 10 Effect of side-to-length (a/b) ratio on the transverse displacement of a GP reinforced concrete slab under different thermal loads ($V_r = 15\%$, $L/h = 10$)

and 20% glass powder reinforced concrete. The panel is simulated using the sinusoidal refined plate theory and assumed to be simply supported and subjected to different linear and non-linear thermal loading across its thickness.

The results of the simulation reveal that the stresses are tensile below the mid-plane ($z/h = 0$) and compressive above the mid-plane for both panels shown in Fig. 11(a) and (b). The axial stress is continuous through the thickness of the slab. Moreover, the results demonstrate a non-linear variation of the axial stress through the thickness of the panel for both cases. The maximum axial stresses are generated by the thermal load ($\bar{T}_3 = 100$).

5 Conclusions

Glass is highly regarded for its recyclability, making it a valuable material in various industries, including construction. In our research, our objective was to investigate the effect of waste glass as nano-powders on the thermomechanical behavior of concrete panels. To achieve this, we conducted an analytical analysis using the refined sinusoidal plate theory to simulate the eco-concrete panel. The efficient Eshelby's homogenization approach was employed to determine the global thermo-elastic properties of the nano-composite. The equations of motion were derived through the application of the principle of virtual work, and the resulting equations were solved using Navier's solutions.

Throughout the study, several factors were considered, including the coefficient of thermal expansion, and mechanical strength of the glass powder reinforced concrete, and based on the thermomechanical analysis conducted on glass powder reinforced concrete, it can be

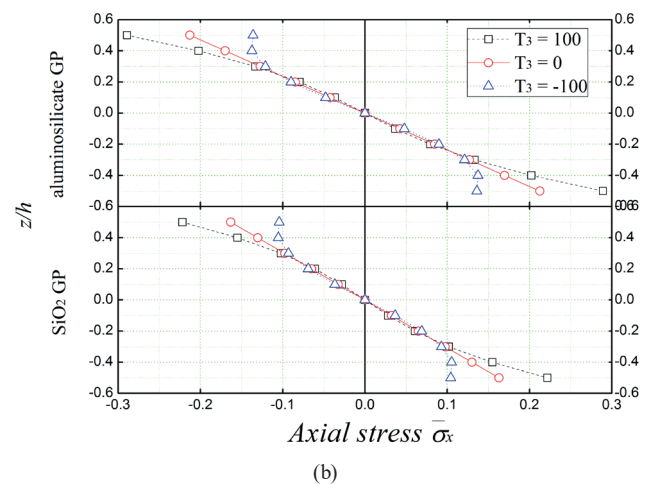
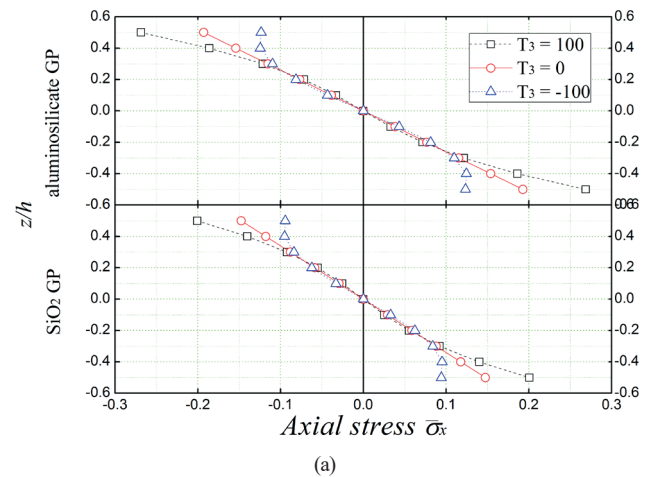


Fig. 11 Variations of dimensionless axial stress through the thickness of square panels under different thermal loadings ($a/h = 5$, $a = b$); (a) $V_r = 5\%$, (b) $V_r = 20\%$

concluded that the use of glass powder as a reinforcement material does not exhibit significant efficiency in enhancing the thermomechanical properties of the concrete.

One possible reason for this inefficiency could be attributed to the relatively low thermal conductivity of glass powder. Concrete typically has higher thermal conductivity than glass powder, resulting in a mismatch between the two materials. This mismatch may limit the effective transfer of heat within the composite material, leading to minimal improvement in the thermomechanical performance. Furthermore, the coefficient of thermal expansion of glass powder may differ from that of the concrete matrix. This difference in coefficients could induce internal stresses during thermal cycling, potentially leading to cracking and reduced mechanical strength of the composite. These factors further contribute to the limited enhancement in thermomechanical behavior observed in the glass powder reinforced concrete.

It is worth noting that while glass powder may not offer substantial benefits in terms of thermomechanical reinforcement, it still possesses other advantageous properties. For instance, glass powder is often used as a partial replacement for cement in concrete mixes due to its pozzolanic activity, which can improve durability and reduce environmental impact.

References

- [1] Du Plessis, C. "A strategic framework for sustainable construction in developing countries", *Construction Management and Economics*, 25(1), pp. 67–76, 2007.
<https://doi.org/10.1080/01446190600601313>
- [2] Naik, T. R. "Sustainability of Concrete Construction", *Practice Periodical on Structural Design and Construction*, 13(2), pp. 98–103, 2008.
[https://doi.org/10.1061/\(ASCE\)1084-0680\(2008\)13:2\(98\)](https://doi.org/10.1061/(ASCE)1084-0680(2008)13:2(98))
- [3] Imbabi, M. S., Carrigan, C., McKenna, S. "Trends and developments in green cement and concrete technology", *International Journal of Sustainable Built Environment*, 1(2), pp. 194–216, 2012.
<https://doi.org/10.1016/j.ijbsbe.2013.05.001>
- [4] Ghareeb, K. S., Ahmed, H. E., El-Affandy, T. H., Deifalla, A. F., El-Sayed, T. A. "The Novelty of Using Glass Powder and Lime Powder for Producing UHPSCC", *Buildings*, 12(5), 684, 2022.
<https://doi.org/10.3390/buildings12050684>
- [5] Sadiqul Islam, G. M., Rahman, M. H., Kazi, N. "Waste glass powder as partial replacement of cement for sustainable concrete practice", *International Journal of Sustainable Built Environment*, 6(1), pp. 37–44, 2017.
<https://doi.org/10.1016/j.ijbsbe.2016.10.005>
- [6] Paul, D., Bindhu, K. R., Matos, A. M., Delgado, J. "Eco-friendly concrete with waste glass powder: A sustainable and circular solution", *Construction and Building Materials*, 355, 129217, 2022.
<https://doi.org/10.1016/j.conbuildmat.2022.129217>
- [7] Hamoudeh, A. R. M., Ikotun, B. D., Babafemi, A. J. "Flexural strength of concrete with recycled fine and coarse crushed glass", *Materials Today: Proceedings*, 86, pp. 32–35, 2023.
<https://doi.org/10.1016/j.matpr.2023.02.089>
- [8] Asgarian, A., Roshan, N., Ghalehnovi, M. "The Strength, Microstructure, and ecological assessment of concrete mix incorporating waste glass powder and polypropylene fiber", *Construction and Building Materials*, 371, 130726, 2023.
<https://doi.org/10.1016/j.conbuildmat.2023.130726>
- [9] Ming, Y., Li, L., Ren, H., Chen, P., Chen, X. "Study on the Binary Hydraulic Kinetics Model of Glass Powder-Cement: Numerical Simulation", *Materials*, 16(5), 1957, 2023.
<https://doi.org/10.3390/ma16051957>
- [10] Raydan, R., Khatib, J., Jahami, A., El Hamoui, A. K., Chamseddine, F. "Prediction of the mechanical strength of concrete containing glass powder as partial cement replacement material", *Innovative Infrastructure Solutions*, 7, 311, 2022.
<https://doi.org/10.1007/s41062-022-00896-8>
- [11] Golafshani, E. M., Kashani, A. "Modeling the compressive strength of concrete containing waste glass using multi-objective automatic regression", *Neural Computing and Applications*, 34, pp. 17107–17127, 2022.
<https://doi.org/10.1007/s00521-022-07360-9>
- [12] de Castro, S., de Brito, J. "Evaluation of the durability of concrete made with crushed glass aggregates", *Journal of Cleaner Production*, 41, pp. 7–14, 2013.
<https://doi.org/10.1016/j.jclepro.2012.09.021>
- [13] Du, H., Tan, K. H. "Properties of high volume glass powder concrete", *Cement and Concrete Composites*, 75, pp. 22–29, 2017.
<https://doi.org/10.1016/j.cemconcomp.2016.10.010>
- [14] Kamali, M., Ghahremaninezhad, A. "Effect of glass powders on the mechanical and durability properties of cementitious materials", *Construction and Building Materials*, 98, pp. 407–416, 2015.
<https://doi.org/10.1016/j.conbuildmat.2015.06.010>
- [15] Nassar, R.-U.-D., Soroushian, P. "Strength and durability of recycled aggregate concrete containing milled glass as partial replacement for cement", *Construction and Building Materials*, 29, pp. 368–377, 2012.
<https://doi.org/10.1016/j.conbuildmat.2011.10.061>
- [16] Ali, E. E., Al-Tersawy, S. H. "Recycled glass as a partial replacement for fine aggregate in self compacting concrete", *Construction and Building Materials*, 35, pp. 785–791, 2012.
<https://doi.org/10.1016/j.conbuildmat.2012.04.117>
- [17] Zhao, H., Poon, C. S., Ling, T. C. "Utilizing recycled cathode ray tube funnel glass sand as river sand replacement in the high-density concrete", *Journal of Cleaner Production*, 51, pp. 184–190, 2013.
<https://doi.org/10.1016/j.jclepro.2013.01.025>
- [18] Eshelby, J. D. "The Determination of the Elastic Field of an Ellipsoidal Inclusion, and Related Problems", *Proceedings of the Royal Society A*, 241(1226), pp. 376–396, 1957.
<https://doi.org/10.1098/rspa.1957.0133>
- [19] Clyne, T. W., Withers, P. J. "An Introduction to Metal Matrix Composites", Cambridge University Press, 1993. ISBN: 978-0511623080
<https://doi.org/10.1017/CBO9780511623080>
- [20] Reddy, J. N. "A simple higher-order theory for laminated composite plates", *Journal of Applied Mechanics*, 51(4), pp. 745–752, 1984.
<https://doi.org/10.1115/1.3167719>
- [21] Touratier, M. "An efficient standard plate theory" *International Journal of Engineering Science*, 29(8), pp. 901–916, 1991.
[https://doi.org/10.1016/0020-7225\(91\)90165-Y](https://doi.org/10.1016/0020-7225(91)90165-Y)

- [22] Karama, M., Afaq, K. S., Mistou, S. "Mechanical behaviour of laminated composite beam by the new multi-layered laminated composite structures model with transverse shear stress continuity", *International Journal of Solids and Structures*, 40, pp. 1525–1546, 2003.
[https://doi.org/10.1016/S0020-7683\(02\)00647-9](https://doi.org/10.1016/S0020-7683(02)00647-9)
- [23] Thai, H.-T., Choi, D.-H. "Improved refined plate theory accounting for effect of thickness stretching in functionally graded plates", *Composites Part B: Engineering*, 56, pp. 705–716, 2014.
<https://doi.org/10.1016/j.compositesb.2013.09.008>
- [24] Zenkour, A. M., Alghamdi, N. A. " Thermoelastic bending analysis of functionally graded sandwich plates", *Journal of Materials Science*, 43, pp. 2574–2589, 2008.
<https://doi.org/10.1007/s10853-008-2476-6>